# COMPARISON OF IMAGING CONDITIONS: APPLICATION TO MARMOUSI DATA

*J. Schleicher, J. C. Costa, and A. Novais*

**email:** *js@ime.unicamp.br*
**keywords:** *Imaging condition, wave-equation migration, amplitude*

## ABSTRACT

*The application of an imaging condition in wave equation shot profile migration is important to provide illumination compensation and amplitude recovery. Particularly for true-amplitude wave-equation migration algorithms, a stable imaging condition is essential to successfully recover the medium reflectivity. We continue our study of a set of image conditions with illumination compensation by application to the Marmousi data. The imaging conditions are evaluated by the quality of the stacked migrated sections. The most stable of the tested imaging condition with illumination compensation divides the crosscorrelation of the up- and downgoing wavefields by the autocorrelation of the downgoing wavefield. Smoothing imaging conditions, which work perfectly in vertically inhomogeneous media, tend to fail for laterally varying velocities.*

## INTRODUCTION

Shot-profile migration is a method used to construct an image of the earth interior from seismic data. This technique is implemented in two steps. The first step consists of downward continuing the source and receiver wavefields for each shot position and the second step consists of applying the imaging condition. The imaging step is based on Claerbout's imaging principle (Claerbout, 1971).

The theoretically correct imaging condition for Claerbout's imaging principle uses one-dimensional deconvolution between the down- and up-going wavefields, i.e., division in the frequency domain. Since this division is unstable off the reflector position, historically, and for practical reasons, the imaging condition is usually estimated by cross-correlating the down- and up-going wavefields (Claerbout, 1971). This yields perfectly stable images since the phase information is correctly preserved and no division is necessary.

However, once migrated amplitudes are another desired result to be obtained from prestack migration, as suggested by Zhang et al. (2003, 2005), a more realistic imaging condition that approximates the division in the frequency domain, needs to be used. Last year, Schleicher et al. (2006) investigated the behaviour of a set of different imaging conditions for a single shot experiment in a simple model that consisted of four horizontal reflectors embedded in a horizontally homogeneous medium with a constant vertical velocity gradient. They concluded that the most stable of the tested imaging conditions with illumination compensation is the one that divides the crosscorrelation of the up- and downgoing wavefields by the autocorrelation of the downgoing wavefield.

In this paper, we carry this analysis to a more realistic situation, comparing the behaviour of the best of the tested imaging conditions when applied to the Marmousi data.

## METHOD

Wave equation migration tries to undo the propagation effects described by the (acoustic) wave equation on the surface data $Q(x_r, y_r; \omega)$ recorded at the receiver at $\mathbf{x}_r = (x_r, y_r, z = 0)$. After Fourier transform,

the wave equation reads

$$\left( \frac{\omega^2}{v^2} + \frac{\partial^2}{\partial z^2} + \Delta \right) p(x, y, z; \omega) = -\delta(\mathbf{x} - \mathbf{x}_s), \tag{1}$$

where $\Delta = \frac{\partial^2}{\partial x^2} + \frac{\partial^2}{\partial y^2}$, and where $\mathbf{x}_s$ denotes the source location. The solution of this equation at $\mathbf{x}_r$ must equal the recorded surface data $Q(x_r, y_r; \omega)$, i.e.,

$$p(x_r, y_r, z = 0; \omega) = Q(x_r, y_r; \omega). \tag{2}$$

To map this solution into depth, the Helmholtz equation (1) is generally decomposed into two one-way wave equations. These are

$$\left( \frac{\partial}{\partial z} + i \frac{\omega}{v} \sqrt{1 + \frac{\omega^2}{v^2} \Delta} \right) P_D = 0, \tag{3}$$

with initial condition

$$P_D(x, y, z = 0; \omega) = \delta(\mathbf{x} - \mathbf{x}_s) \tag{4}$$

for the downgoing waves, and

$$\left( \frac{\partial}{\partial z} - i \frac{\omega}{v} \sqrt{1 + \frac{\omega^2}{v^2} \Delta} \right) P_U = 0 \tag{5}$$

with initial condition

$$P_U(x, y, z = 0; \omega) = Q(x, y; \omega) \tag{6}$$

for the upgoing waves.

After propagating the waves from the indicated initial conditions at $z = 0$ into the underground (downgoing waves forward from $t = 0$, upgoing waves backward from $t = t_{\max}$), an imaging condition must be applied in order to obtain the final image. The theoretically correct imaging condition is the division of both wavefields at the reflectors depth in order to recover the reflection coefficient as the amplitude ratio, i.e.,

$$R(x, y, z) = \sum_{j=1}^{N_\omega} \frac{P_U(x, y, z; \omega_j)}{P_D(x, y, z; \omega_j)} , \tag{7}$$

where $N_\omega$ is the number of frequencies used in the process. Since the reflector position is unknown, this division has to be carried out at all depths, which is rather unstable, because the downgoing wavefield will be zero at some places. Therefore, some stabilization is required. For this purpose, many different practical imaging conditions have been suggested. Below we give an overview over a number of them and compare their performance on a simple vertical-gradient model with four horizontal interfaces, as well as the Marmousi data.

## IMAGING CONDITIONS

### Crosscorrelation

The simplest imaging condition is the one originally proposed by Claerbout (1971). It uses a simple convolution of the up- and downgoing fields, viz.

$$R(x, y, z) = \sum_{j=1}^{N_\omega} P_D^*(x, y, z; \omega_j) P_U(x, y, z; \omega_j), \tag{8}$$

where the asterisk denotes the complex conjugate.

This condition is obtained as a simplification of

$$R(x, y, z) = \sum_{j=1}^{N_\omega} \frac{P_U(x, y, z; \omega_j) P_D^*(x, y, z; \omega_j)}{P_D(x, y, z; \omega_j) P_D^*(x, y, z; \omega_j)} , \tag{9}$$

which is obtained from equation (7) by multiplication of numerator and denominator with $P_D^*(x, y, z; \omega_j)$, in order to make the denominator real. Of course, equation (9) does not remedy the division by zero. However, the denominator is now merely a scale factor that does no longer contain any phase information. Thus, if no amplitude information is to be preserved, the denominator can be omitted, leading to imaging condition (8).

**Stabilized divisions**

Actual implementations of imaging condition (9) retaining the denominator need to apply some stabilization. Here, we have tested two forms. The first one is an additive form, given by

$$R(x, y, z) = \sum_{j=1}^{N_\omega} \frac{P_U(x, y, z; \omega_j) P_D^*(x, y, z; \omega_j)}{P_D(x, y, z; \omega_j) P_D^*(x, y, z; \omega_j) + \varepsilon} \; , \qquad (10)$$

where $\varepsilon$ is an additive constant. There are many ways to define its value. A constant value for all depth levels is generally an inadequate choice, leading to insufficient stability or too strong smoothing at different depth levels. In our numerical tests, we used

$$\varepsilon = \varepsilon(\omega, z) = \lambda[\max_{x,y}(|P_D(x, y, z; \omega)|^2)] \; . \qquad (11)$$

In other words, the stabilization is achieved by adding a fraction ($0 < \lambda < 1$) of the maximum of the squared absolute value of the downgoing wavefield at the current depth level to the denominator.

The second one is a low-cut form, given by

$$R(x, y, z) = \sum_{j=1}^{N_\omega} F(x, y, z; \omega_j), \qquad (12)$$

where

$$F(x, y, z; \omega) = \begin{cases} \dfrac{P_U(x, y, z; \omega_j) P_D^*(x, y, z; \omega)}{P_D(x, y, z; \omega) P_D^*(x, y, z; \omega)}, & \text{if } |P_D(x, y, z; \omega)|^2 > \varepsilon \\ 0 & \text{otherwise} \end{cases} \; , \qquad (13)$$

where $\varepsilon$ is again defined by equation (11). In other words, stabilization is achieved by substitution of all values of the denominator smaller than a fraction of the maximum value of the wavefield at the current depth level by that value.

Since the corresponding stabilization of the the original complex division 7 already turned out to be of very poor quality, we refrained from testing it on the Marmousi data.

**Smoothing**

Recently, imaging conditions using lateral smoothing have been proposed (Guitton et al., 2006). We have tested four such conditions. The first one uses a smoothed denominator in equation (9), i.e.,

$$R(x, y, z) = \sum_{j=1}^{N_\omega} \frac{P_U(x, y, z; \omega_j) P_D^*(x, y, z; \omega_j)}{<P_D(x, y, z; \omega_j) P_D^*(x, y, z; \omega_j)>} \; , \qquad (14)$$

where the smoothing operator is

$$<P_D(x_i, y_k, z; \omega) P_D^*(x_i, y_k, z; \omega)> = \sum_{l=i-n_x}^{i+n_x} \sum_{m=k-n_y}^{k+n_y} P_D(x_l, y_m, z; \omega) P_D^*(x_l, y_m, z; \omega) \; . \qquad (15)$$

Here $n_x$ and $n_y$ represent the size of the smoothing windows in the $x$ and $y$ directions.

The next imaging condition uses corresponding smoothing also in the numerator. In formulas,

$$R(x,y,z) = \sum_{j=1}^{N_\omega} \frac{<P_U(x,y,z;\omega_j)P_D^*(x,y,z;\omega_j)>}{<P_D(x,y,z;\omega_j)P_D^*(x,y,z;\omega_j)>} \; . \tag{16}$$

The other two smoothing imaging condition add another smoothing operation along the frequency axis to the lateral smoothing as indicated above. These conditions read

$$R(x,y,z) = \sum_{j=1}^{N_\omega} \frac{P_U(x,y,z;\omega_j)P_D^*(x,y,z;\omega_j)}{\ll P_D(x,y,z;\omega_j)P_D^*(x,y,z;\omega_j)\gg} \tag{17}$$

and

$$R(x,y,z) = \sum_{j=1}^{N_\omega} \frac{\ll P_U(x,y,z;\omega_j)P_D^*(x,y,z;\omega_j)\gg}{\ll P_D(x,y,z;\omega_j)P_D^*(x,y,z;\omega_j)\gg} \; . \tag{18}$$

where the smoothing operator now also contains a sum in $\omega$, i.e.,

$$\ll P_D(x_i,y_k,z;\omega_s)P_D^*(x_i,y_k,z;\omega_s)\gg = \sum_{l=i-n_x}^{i+n_x} \sum_{m=k-n_y}^{k+n_y} \sum_{t=s-n_\omega}^{s+n_\omega} P_D(x_l,y_m,z;\omega_t)P_D^*(x_l,y_m,z;\omega_t) \; . \tag{19}$$

Here $n_x$, $n_y$, and $n_\omega$ represent the size of the smoothing windows in the $x$, $y$, and $\omega$ directions, respectively.

**Division by autocorrelation**

In the single-shot examples of Schleicher et al. (2006), to divide the complete crosscorrelation of the up- and downgoing wavefields at the current depth level at $t = 0$ by the autocorrelation of the downgoing wavefield turned out to be the most stable of the tested imaging conditions with illumination compensation. In symbols, this image condition reads

$$R(x,y,z) = \frac{U(x,y,z)}{D(x,y,z)} \; , \tag{20}$$

where

$$U(x,y,z) = \sum_{j=1}^{N_\omega} P_U(x,y,z;\omega_j)P_D^*(x,y,z;\omega_j) \tag{21}$$

and

$$D(x,y,z) = \sum_{j=1}^{N_\omega} P_D(x,y,z;\omega_j)P_D^*(x,y,z;\omega_j) \; . \tag{22}$$

This imaging condition is the result of a least-squares inversion of the equation

$$P_U(x,y,z;\omega) = R(x,y,z)P_D(x,y,z;\omega) \tag{23}$$

for all $\omega$ (Arienti et al., 2002). Equation (23) relates the up- and downgoing fields at the image point. In other words, $R(x,y,z)$ of equation (20) minimizes the cost function

$$C(R(x,y,z)) = \frac{1}{2} \sum_{j=1}^{N_\omega} [P_U(x,y,z;\omega) - R(x,y,z)P_D(x,y,z;\omega)]^2 \; . \tag{24}$$

It turns out that equation (20) is a rather stable imaging condition. Only at the corners of the migrated image, very far from sources and receivers, some problems may occur. Because of the location of these
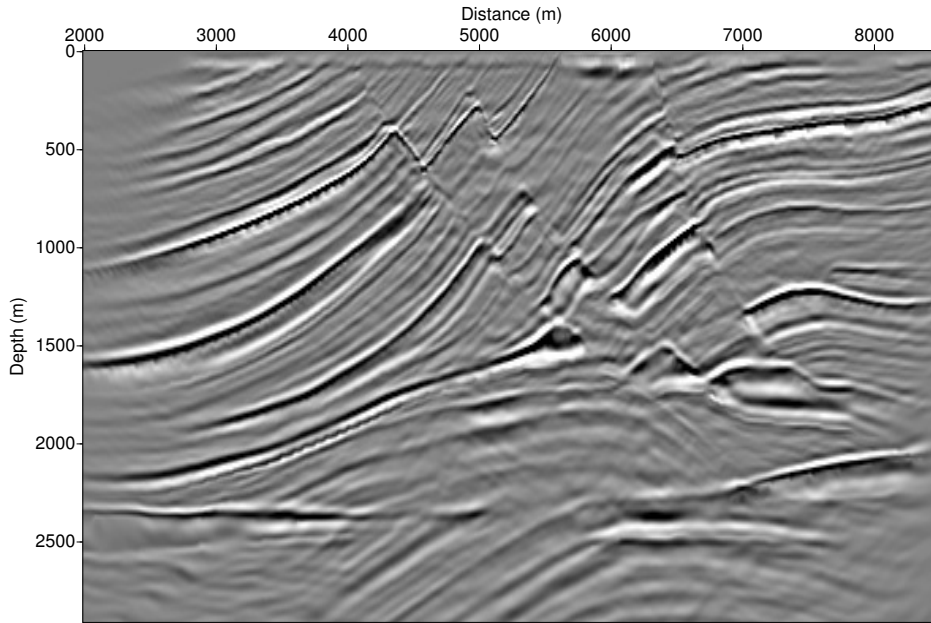
**Figure 1:** Marmousi data migrated using the crosscorrelation imaging condition.

problems, it is sufficient to avoid these areas. Thus, for the application to the Marmousi data, we have tested the slightly modified forms

$$R(x,y,z) = \frac{U(x,y,z)}{D(x,y,z) + \varepsilon} \; , \tag{25}$$

and

$$P(x,y,z;\omega) = \begin{cases} \dfrac{U(x,y,z)}{D(x,y,z)}, & \text{if } |D(x,y,z)| > \varepsilon \\ 0 & \text{otherwise} , \end{cases} \tag{26}$$

where

$$\varepsilon = \varepsilon(z) = \max\{\alpha, \lambda \max_{x,y}(|D(x,y,z;\omega)|)\} \; . \tag{27}$$

Note that conditions (20) and (26) can be easily generalized to incorporate the time-shift imaging condition of Sava and Fomel (2006). All that needs to be done is calculation of the inverse Fourier transforms in the numerator and denominator with opposite time shifts.

### NUMERICAL EXPERIMENTS

**Marmousi data**

To study the quality of the best of the above imaging conditions under more realistic conditions, we applied them to the Marmousi data (Versteeg, 1994). The employed migration was a common-shot PSPI migration with ten reference velocities chosen according to the maximum entropy criterion of Bagaini et al. (1995). The following figures depict the resulting depth-migrated image using the true velocity distribution. Note that we used the same migration in all cases, only varying the imaging condition, thus eliminating the influence of migration from the image variations. Therefore, all differences in the images below are a direct concequence of the different imaging conditions used.

**Crosscorrelation.—**    Figure 1 shows the migration result for the standard crosscorrelation imaging condition. This image should be considered a benchmark, since the applied imaging conditions are not supposed to degrade the image quality in comparison to this one.
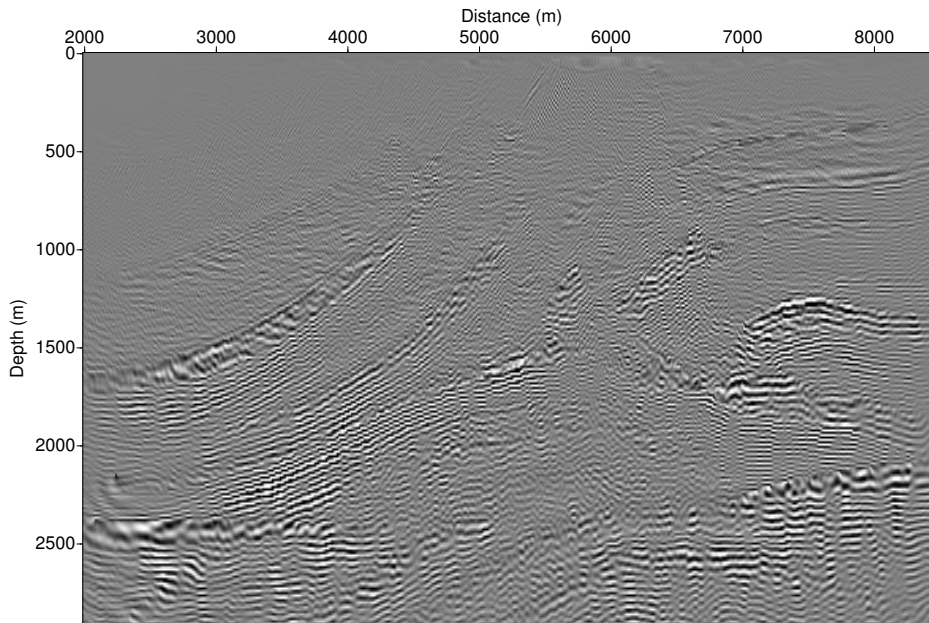
**Figure 2:** Marmousi data migrated using the imaging condition by stabilized division [equation (10)] using the variable $\varepsilon$ of equation (11) with $\lambda = 0.1$.

**Stabilized divisions.—** The first imaging condition with illumination compensation to be tested is the stabilized division of equation (10) (see Figure 2). As we know from the tests of Schleicher et al. (2006), divisional imaging conditions tend to create migration artifacts. This becomes immediately clear when we compare Figure 2 to Figure 1. The migration artifacts are so strong that the actual image cannot be seen except for a few very strong reflectors. Figure 4 was obtained using $\lambda = 0.1$ in equation (11). However, increasing $\lambda$ does not much to improve the situation. This can be seen in Figure 3, which was obtained with $\lambda = 0.2$.

Actual stabilization could only be achieved using quite a large fixed value for $\varepsilon$ of $10^{-4}$ for the whole migration of all shots at all depths rather than a variable $\varepsilon$ with depth as suggested in connection with condition (10). The result is depicted in Figure 4. We note that the images in Figures 1 and 4 look almost identical. The reason is the large stabilization value, which makes the illumination compensation almost a division by a constant scale factor, thus resulting in no relative differences between the images.

The situation is almost identical if we avoid adding $\varepsilon$ to the denominator but carry out the division only if the denominator exceeds $\varepsilon$ as proposed in imaging condition (12). For $\lambda = 0.1$ and $\lambda = 0.2$, we obtain the images of Figures 5 and 6, respectively. By substitution for a fixed $\varepsilon = 10^{-4}$, the image improves again, though it remains full of artifacts (see Figure 7).

### Smoothing

The results of the imaging conditions (14) to (18) that rely on smoothing are depicted in the next figures. Figures 8 and 9 show the results of condition (14), which smoothes the denominator of the division, for two different sizes of the smoothing window, $n_x = 75$ and $n_x = 256$. The structure of the image has improved in comparison to the images in Figures 2, 3, 5, 6, and even 7. Moreover, the illumination compensation can be seen to have an effect as the stronger reflections deeper in the model like, for instance, the reservoir reflections, have stronger amplitudes as before. However, the migration artifacts are still rather strong, deteriorating the image quality. The effect of the different window sizes is barely detectable.
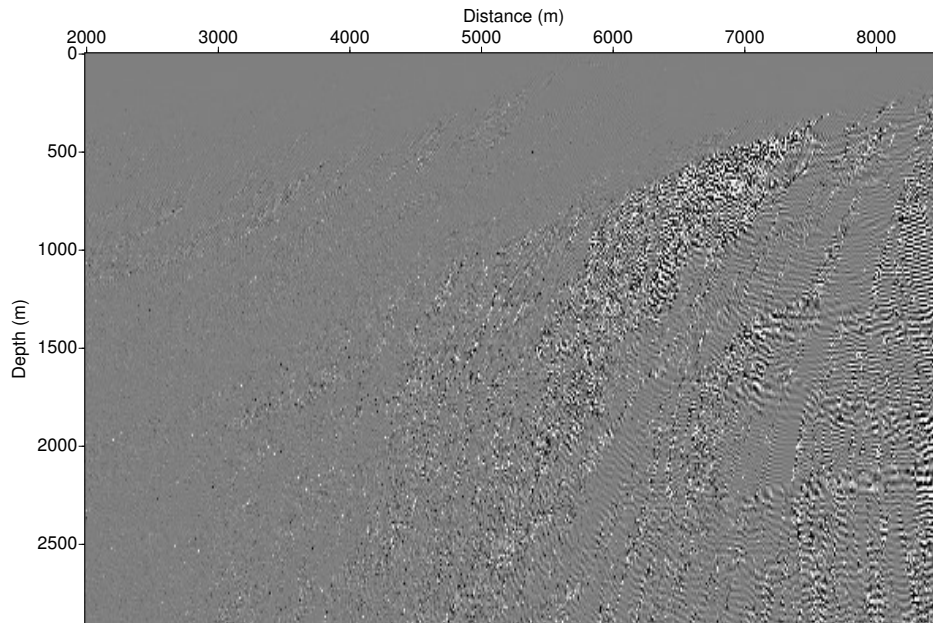
The behaviour of condition (16), which smoothes the both the numerator and the denominator, is quite
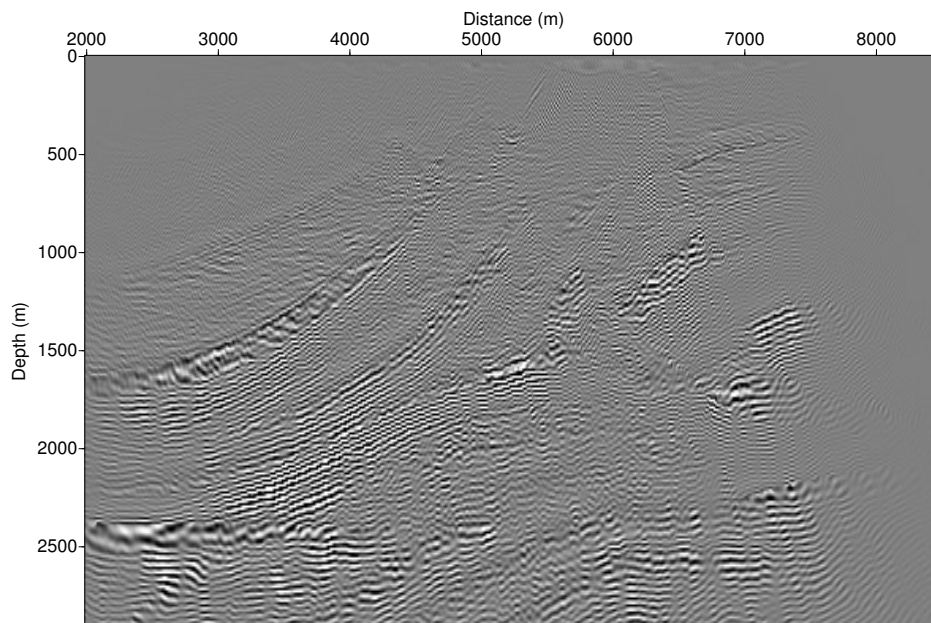
**Figure 3:** Marmousi data migrated using the imaging condition by stabilized division [equation (10)] using the variable $\varepsilon$ of equation (11) with $\lambda = 0.2$.
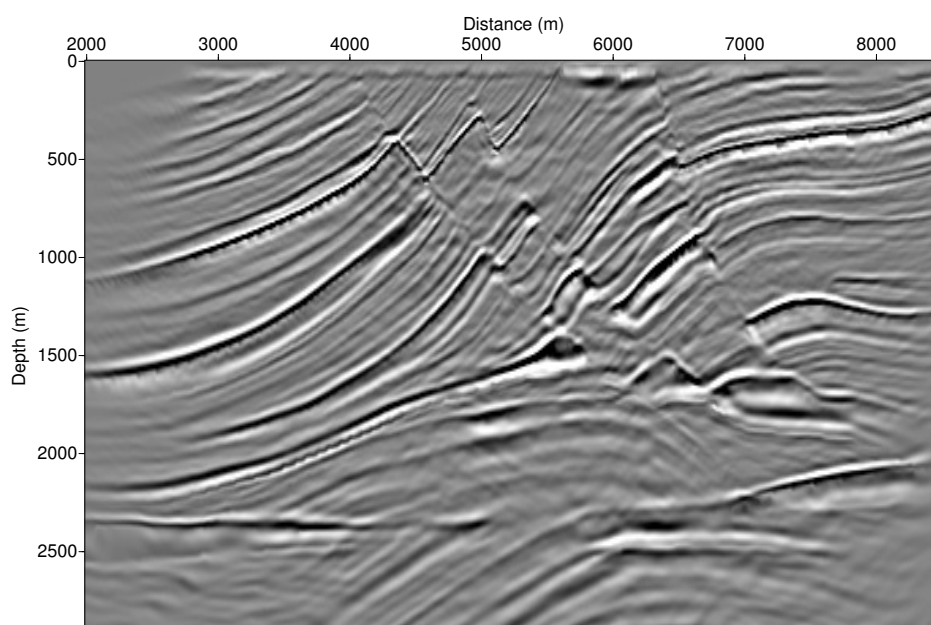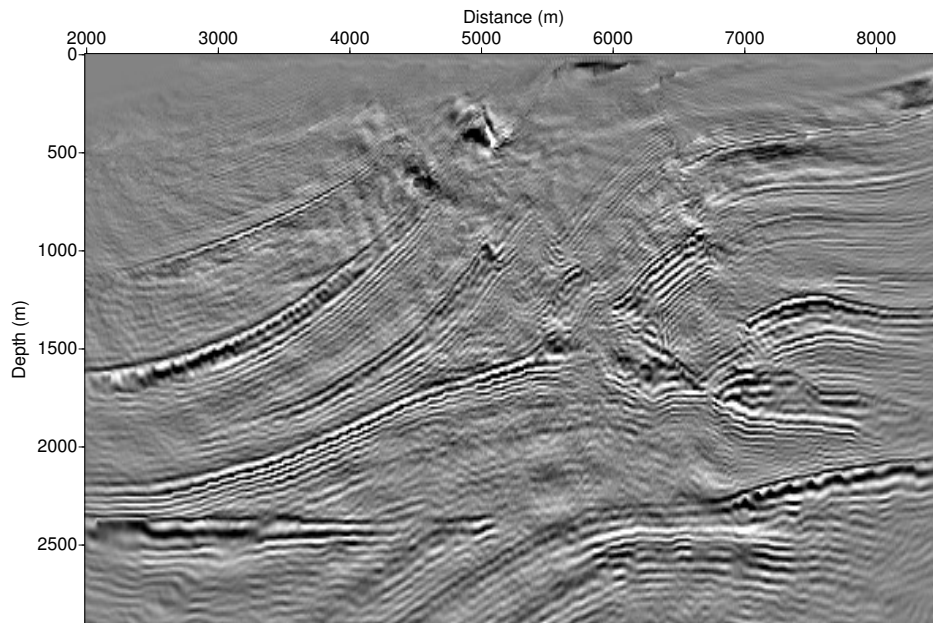


**Figure 4:** Marmousi data migrated using the imaging condition by stabilized division [equation (10)] using a fixed $\varepsilon = 10^{-4}$.
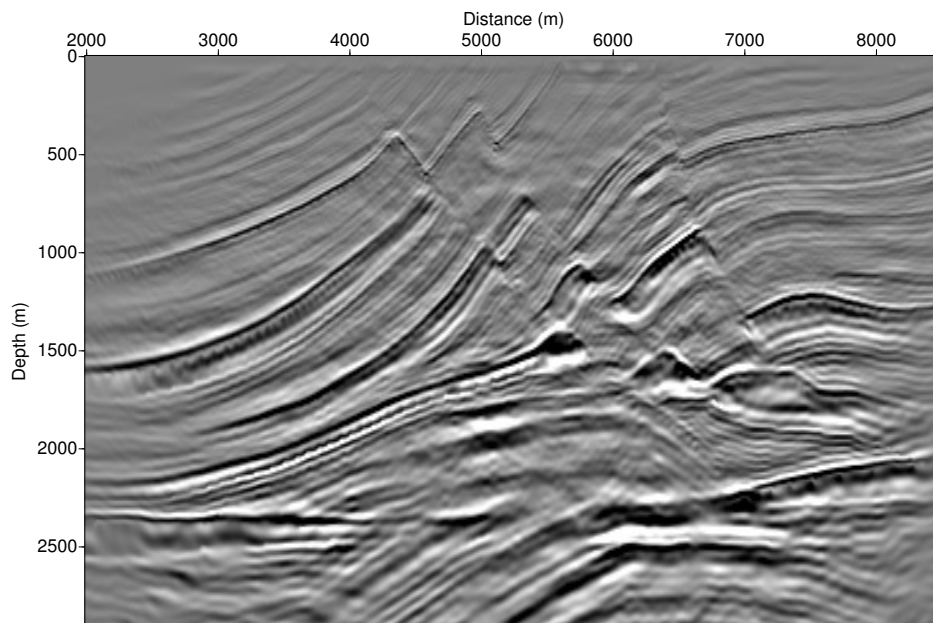
**Figure 5:** Marmousi data migrated using the imaging condition by stabilized division [equation (12)] using the variable $\varepsilon$ of equation (11) with $\lambda = 0.1$.
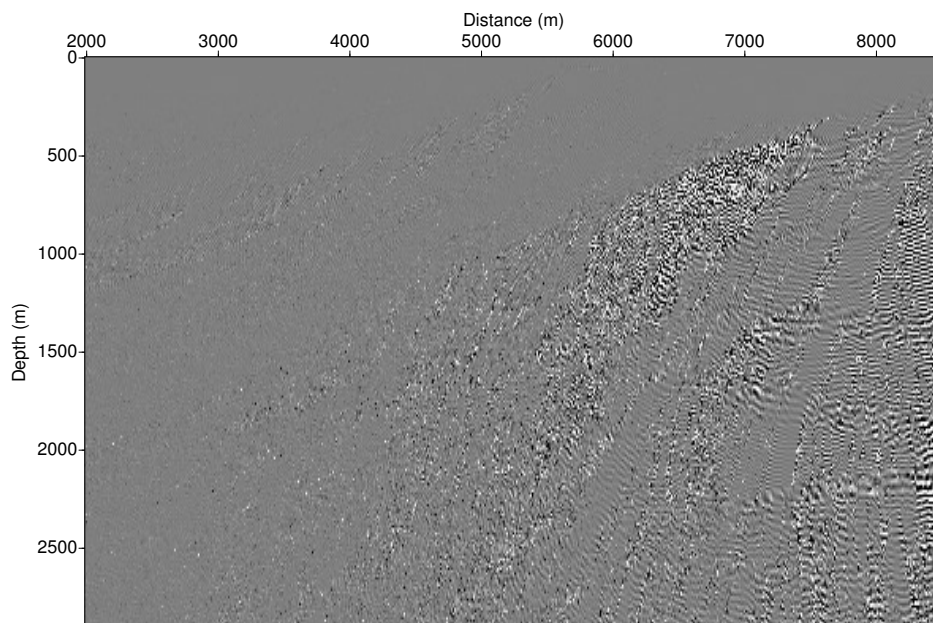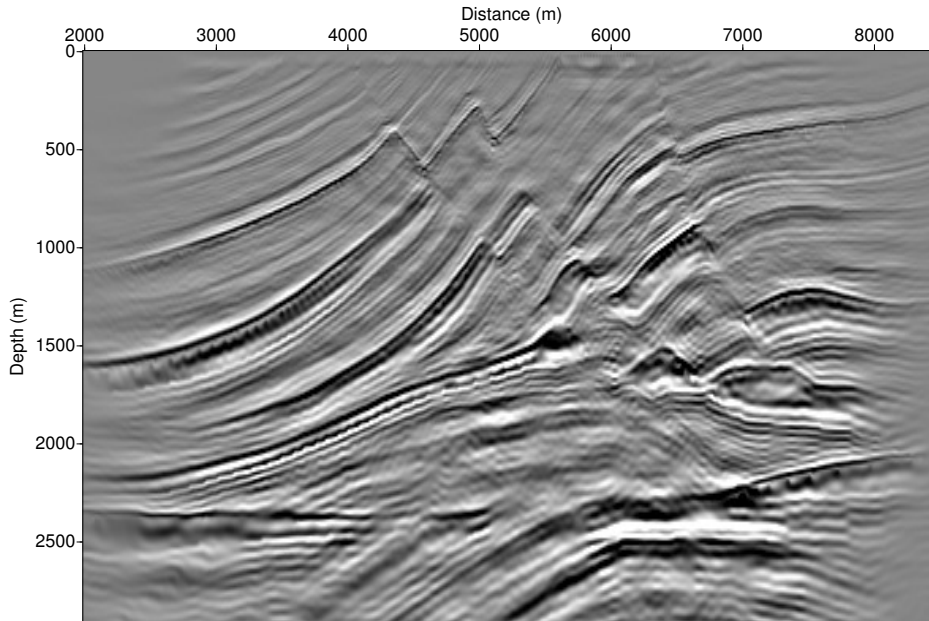


**Figure 6:** Marmousi data migrated using the imaging condition by stabilized division [equation (12)] using the variable $\varepsilon$ of equation (11) with $\lambda = 0.2$.

**Figure 7:** Marmousi data migrated using the imaging condition by stabilized division [equation (12)] using a fixed $\varepsilon = 10^{-4}$.



**Figure 8:** Marmousi data migrated using the imaging condition with lateral denominator smoothing [equation (14)] with a window size of $n_x = 75$.

**Figure 9:** Marmousi data migrated using the imaging condition with lateral denominator smoothing [equation (14)] with a window size of $n_x = 256$.

different (see Figure 10 for a window size for the smoothing operator of $n_x = 150$). Because the smoothing is applied horizontally, not following the geological structure, the numerator smoothing leads to strong horizontal smear in the image, obscuring any structural information, even with a rather short smoothing operator with $n_x = 75$..

The corresponding images for condition (17) are shown in Figures 11 and 12, again for two two sizes of the lateral smoothing window of $n_x = 128$ and $n_x = 256$, with a rather short frequency smoothing window of $n_\omega = 10$. Again, the influence of the window size is irrecognizable. We note that while the structure of the Marmousi model can be guessed, the migration noise is still unacceptably strong. We conclude that contrary to the observation for the vertically inhomogeneous medium, frequency smoothing in complex media does not help to improve the image. We refrain from including a figure for condition (18), since it is rather obvious that smoothing in frequency in addition to the lateral smoothing already applied in Figure 10 won't do any good.

In summary, our numerical tests with lateral smoothing imaging conditions for the Marmousi data exclusively yielded unsatisfactory results. Numerator smoothing smears the image since the smoothing generally does not follow reflectors as in the case of the above simple model. Smoothing the denominator alone was only slightly better. However, even when choosing a rather large size for the smoothing filter, division by zero could not be avoided for certain frequencies, resulting in very unstable images. A possible remedy might be the omission of frequencies that cause denominators close to zero. Those frequencies should be removable without degrading the image as the do not carry any extractable information anyway.

**Division by autocorrelation**

Finally, Figures 13, 14, and 15 show the results of imaging conditions (20), (25), and (26), respectively, that division of the crosscorrelation by the autocorrelation. For conditions (25) and (26), we chose $\lambda = 0.05$ and $\alpha = 10^{-6}$ in equation (27). Note that for the stack, each migrated shot had to be normalized by its rms value so as to guarantee comparable energy in each image.

As expected, the artifacts outside the illuminated regions perturb the image obtained with the uncondi-
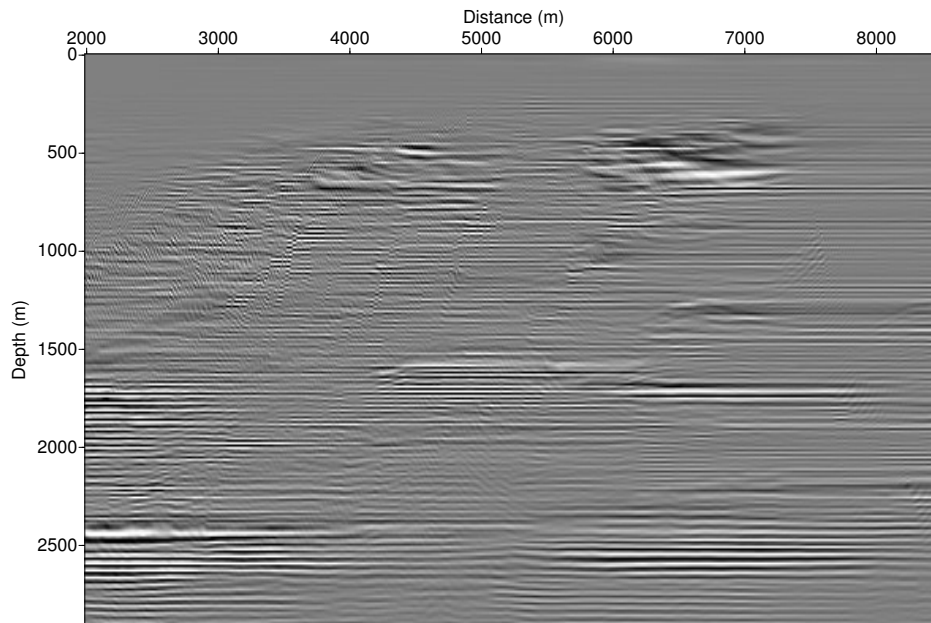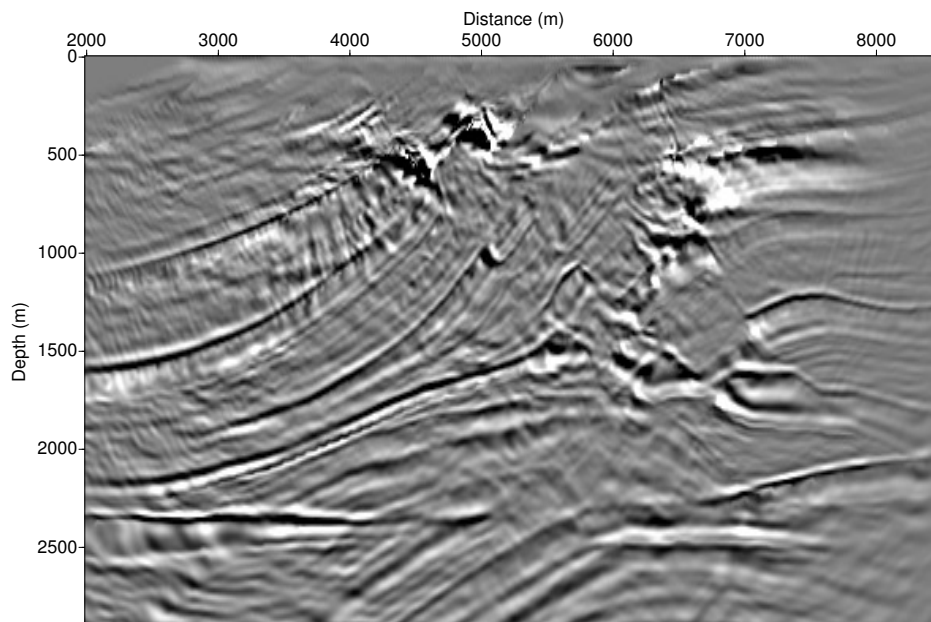
**Figure 10:** Marmousi data migrated using the imaging condition with lateral numerator and denominator smoothing [equation (16)].
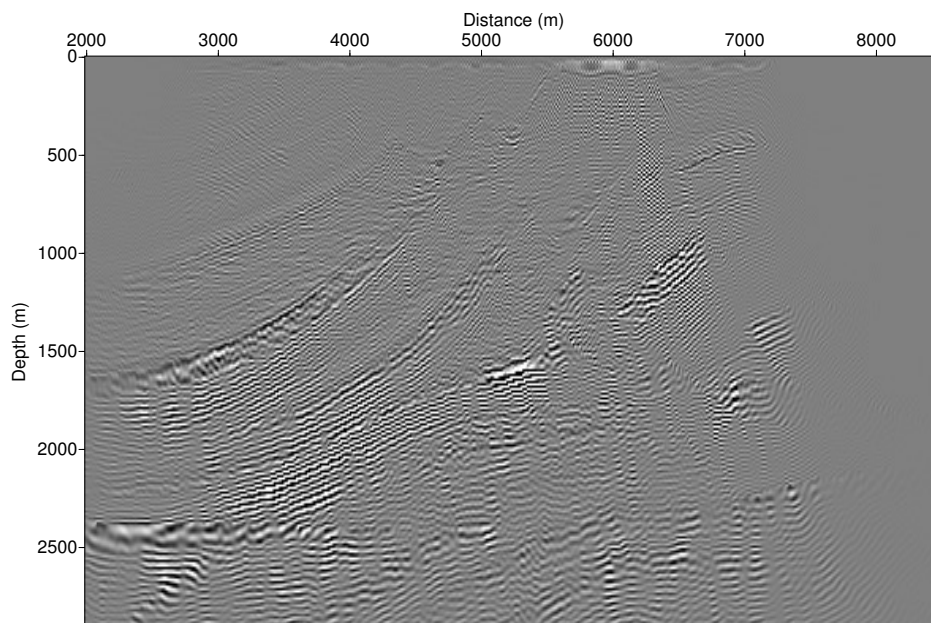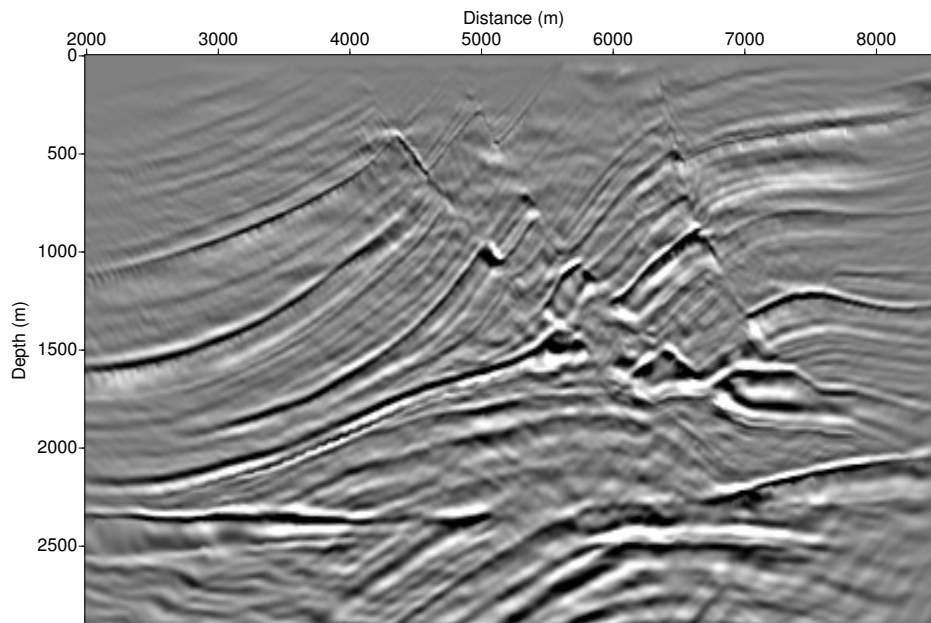


**Figure 11:** Marmousi data migrated using the imaging condition with lateral and frequency denominator smoothing [equation (16)] with a window size of $n_x = 128$ and $n_\omega = 10$.
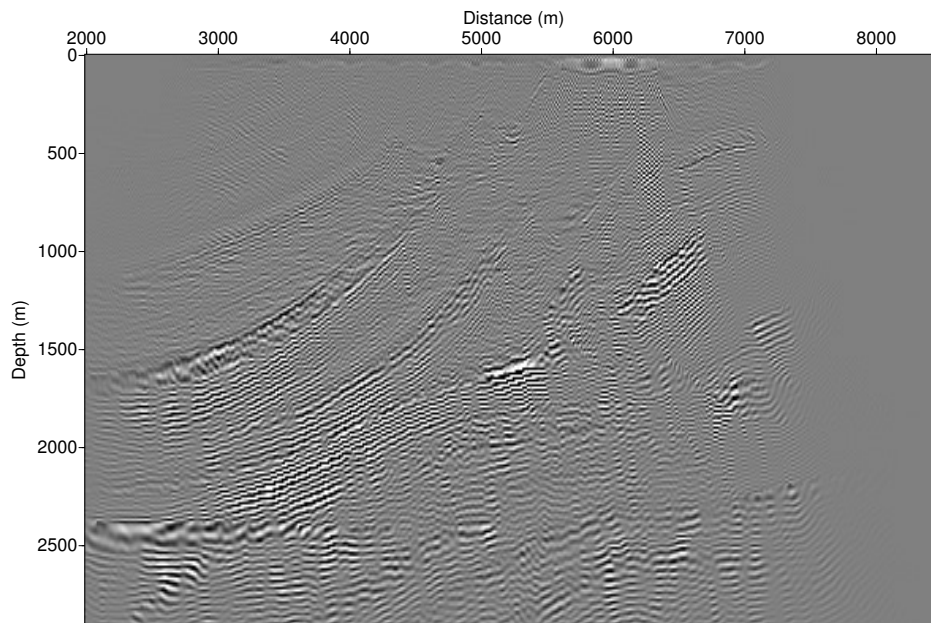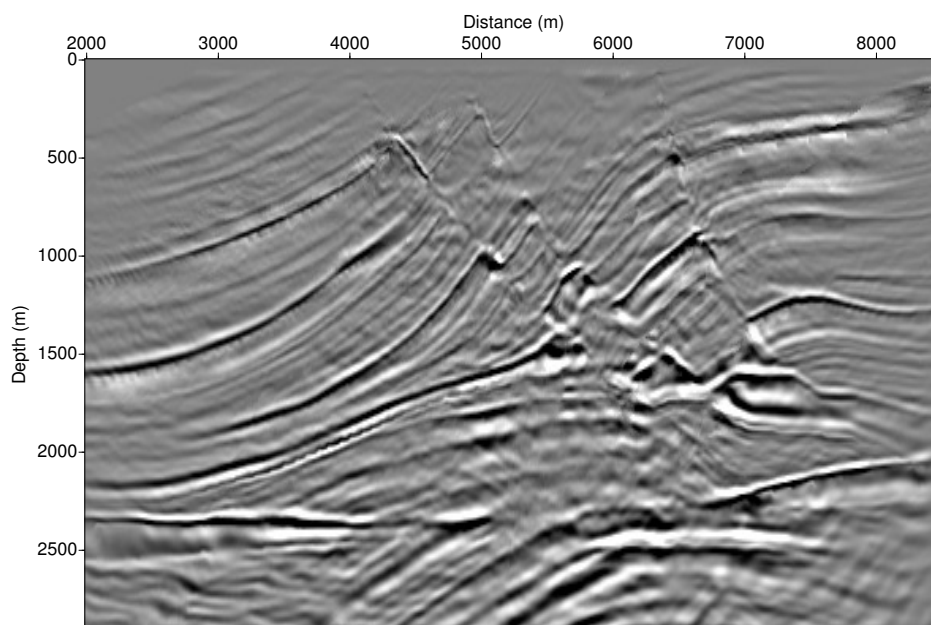
**Figure 12:** Marmousi data migrated using the imaging condition with lateral and frequency denominator smoothing [equation (16)] with a window size of $n_x = 256$ and $n_\omega = 10$.



**Figure 13:** Marmousi data migrated using the imaging condition dividing the crosscorrelation by the autocorrelation.

**Figure 14:** Marmousi data migrated using the imaging condition dividing the crosscorrelation by the stabilized autocorrelation.



**Figure 15:** Marmousi data migrated using the imaging condition (26) dividing the crosscorrelation by the nonzero autocorrelation.

tional application according to equation (20). However, both modified divisions (25) and (26) produce very nice results. Figure 14 shows the result of stabilizing the division by adding a small $\varepsilon$ to the autocorrelation (equation 25). In Figure 15, we see the result of its conditional form 26, which applies the division only where the autocorrelation is larger than a small threshold value. In both cases we have used a very small value given in equation (27) with $\lambda = 0.05$. Both migrated images are virtually identical to each other, showing an improved recovery of the reservoir zone when compared to the simple crosscorrelation result. Overall, the strength of the reflector images resemble more closely the relative strength of the contrasts in the original Marmousi model.

Upon a very close inspection some minor differences can be spotted between Figures 14 and 15. While the conditional autocorrelation division (Figure 15) resolves some details in the fault region a little better, it loses a bit of continuity of the two reflectors below the fault zone. Also, its resolution of the strongest reflector in the top right corner is a bit reduced in comparison to the stabilized autocorrelation division (Figure 14).

As expected from the single-shot experiments of Schleicher et al. (2006), setting the image to zero where the downgoing wavefield is too small actually provides a nice muting of undesired effects outside the actual image. Note that although image conditions 20, 25, and 26 carry out the illumination compensation by division with the downgoing wavefield, the migration artifacts in Figures 14 and 15 are not worse than those of Claerbout's simple convolutional image condition (8) in Figure 1.

## CONCLUSIONS

If the amplitudes of wave-equation migration are to be corrected for geometrical-spreading effects in heterogeneous media, it is important to take the effect of the imaging condition into account. Different imaging conditions have different effects on the resulting migrated images. Divisional imaging conditions generally strongly enhance migration artifacts. Standard stabilization techniques may lead to altered reflection amplitudes.

In this paper, we have compared the numerical behaviour of a number of different imaging conditions for common-shot wave equation migration when applied to the Marmousi data. As in the previous tests using a single shot from a vertical-gradient model with four horizontal interfaces, the most stable of the tested imaging condition with illumination compensation turned out to be the one that divides the cross-correlation of the up- and downgoing wavefields by the autocorrelation of the downgoing wavefield. In this way, not only the migration artifacts are strongly reduced, but the amplitudes become more stable and reliable.

Our tests on the Marmousi data demonstrated that an application of the latter imaging condition can help to preserve relative amplitudes of reflectors, i.e., strong or weak velocity contrasts in the earth appear as strong or weak reflections in the image, respectively. The muting of images where the downgoing field is close to zero was successful for the cited imaging condition to reduce migration artifacts outside the illuminated area.

## ACKNOWLEDGMENTS

## REFERENCES

Arienti, M. T., Bonomi, E., Cardone, G., and Cazzola, L. (2002). Amplitude-preserving Monte Carlo 3D prestack migration. In *64th EAGE Conference and Exhibition, Expanded Abstracts*, pages B09:1–4, Florence, Italy. EAGE.

Bagaini, C., Bonomi, E., and Pieroni, E. (1995). Split convolutional approach to 3-d depth extrapolation. In *65th Annual International Meeting, SEG, Expanded Abstracts*, pages 195–198.

Claerbout, J. F. (1971). Toward a unified theory of reflector mapping. *Geophysics*, 36(3):467–481.

Guitton, A., Valenciano, A., and Bevc, D. (2006). Robust imaging condition for shot profile migration. In *Expanded Abstracts, 76rd Annual International Meeting*, pages 1059–1062. Soc. of Expl. Geophys.

Sava, P. and Fomel, S. (2006). Time-shift imaging condition on seismic migration. *Geophysics*, 71(6):S209–S217.

Schleicher, J., Costa, J. C., and Novais, A. (2006). A comparison of imaging conditions for wave-equation shot-profile migration. *Annual WIT Report*, 10:118–130.

Versteeg, R. (1994). The marmousi experience: Velocity model determination on a synthetic complex data set. *The Leading Edge*, 13:927–936.

Zhang, Y., Zhang, G., and Bleistein, N. (2003). True amplitude wave equation migration arising from true amplitude one-way wave equations. *Inverse Problems*, 19:1113–1138.

Zhang, Y., Zhang, G., and Bleistein, N. (2005). Theory of true-amplitude one-way wave equations and true-amplitude common-shot migration. *Geophysics*, 70(4):E1–E10.